

# High performance finite element analysis of composite aeroelastic structures

A. Maheri & A. Daadbin

*School of Computing, Engineering and Information Sciences,  
Northumbria University, UK*

## Abstract

A high performance finite element analysis software tool has been developed for high fidelity deformation analysis of aeroelastic tailored wings and blades made of anisotropic composite materials. The package comprises an in-line semi-automatic adaptive mesh generator and a finite element solver. An aerodynamic solver can be plugged into the package to perform a coupled aero-structure analysis. The finite element solver employs a natural-mode triangular shell element, yielding accurate results with high convergence rate in deformation analysis of thin and moderately thick composite shell structures. In mesh generation, the aerodynamic and structural characteristics of the aeroelastic structure directly influence the domain discretization procedure. It has been shown that a mesh generated based on this algorithm has significant effect on improving the convergence rate of results.

*Keywords: FEA, mesh generation, elastic coupling, anisotropic composites, aeroelastic tailoring, anisotropic mesh, adaptive blade, smart wing.*

## 1 Introduction

Mainly due to their high strength-weight ratio and good fatigue life, fibrous composite materials have found a vast range of applications. More recently, another feature of these materials has been receiving great attention with proven or potential applications in the field of smart and adaptive lightweight aerostructures. Aerodynamic surfaces made of fibrous composites can be aeroelastically tailored. An implanted elastic coupling, due to a planned lay-up and fibre orientations, can have a favourable influence on the aerodynamic



performance of the aerodynamic surface, e.g. passive load alleviation in smart wings and wind turbine blades that are adaptive to the operating condition [1, 2].

The design of aeroelastic wings and blades is different from the design of conventional wings and blades in three ways. (i) The aerodynamic design of adaptive blades or smart wings cannot be carried out without having sufficient knowledge about their material properties and structural characteristics while, in the case of conventional wings and blades, the aerodynamic design can be independently performed prior to the structural design. This makes the aerodynamic and structural designs of these aerodynamic surfaces integrated in nature. (ii) Adaptive blades and smart wings have dynamic topologies that vary with operating condition. Hence, the current practice for topology design of conventional aerodynamic surfaces is no longer applicable to aeroelastic surfaces. Their design is rather a search-based design. Performing a search-based integrated design requires efficient analysis tools. (iii) Aeroelastic blades and wings act as open loop control systems and need to be designed to function optimally over a range of operating conditions. That is, variation of surface topology due to the presence of elastic coupling (referred to as induced deformation) must also be considered, directly or indirectly, as a design variable.

The magnitude of the induced deformation, its span-wise variation and its response to the variation of operating condition, depends on the aerodynamic and structural characteristics of the aeroelastic surface as well as the operating condition itself. In order to evaluate the aerodynamic performance of an aeroelastic surface, a structural analyser is required to predict the induced deformation accurately. The fact that even small changes in the topology of an aerodynamic surface could have significant effects on its aerodynamic performance, together with the current deficiencies in the available analytical models in analysis of anisotropic composites, have placed the finite element (FE) techniques to the fore of structural analysis of aeroelastic surfaces.

Additional complexity arises due to the interaction between the topology of the aeroelastic surface and the applied aerodynamic loads. This interaction makes the analysis of these structures iterative by nature [2]. That is, an iterative coupled aero-structure analysis must be carried out at each given operating condition. In a coupled aero-structure analysis, the effect of the induced deformation on the surface topology is taken into account. Correcting the surface topology, its effect on the aerodynamic loading and induced deformation will be re-calculated. This sequence repeats until a converged solution has been achieved. A schematic description of a coupled aero-structure analysis is shown in Figure 1.

Running a finite element analysis (FEA) within an iteration loop can be very time consuming. In the case of aeroelastic surfaces, in which the search-based design process requires hundreds of objective evaluations, employing a coupled aero-structure analysis can be extremely time consuming. Since the topology of the aeroelastic surface changes from one iteration to another, in each iteration a new mesh must be generated and then the aerodynamic loads must be updated and re-distributed accordingly. In fact, in each aero-structure iteration a complete mesh refinement process should be carried out unless the initial mesh

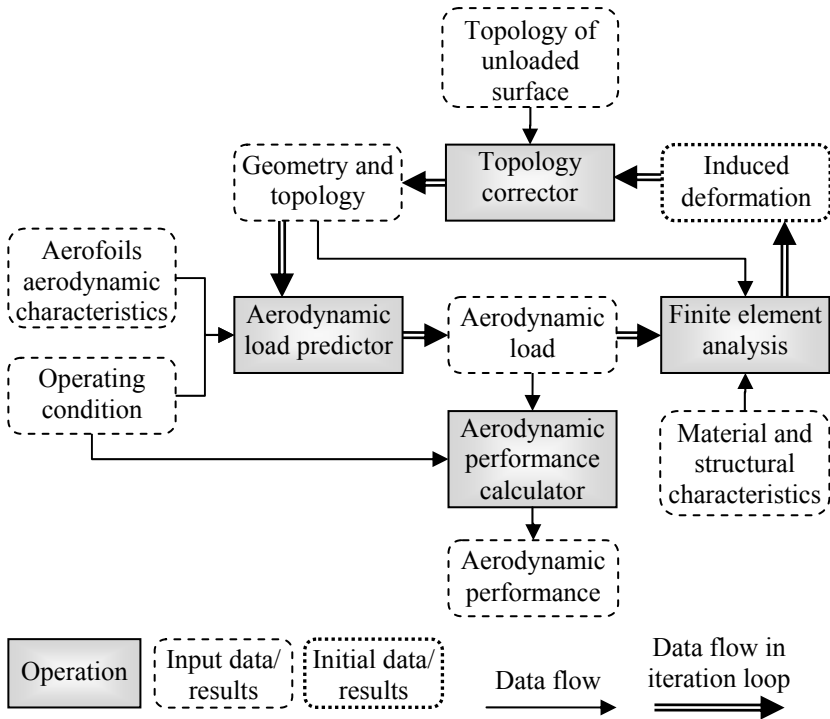


Figure 1: Coupled aero-structure analysis of an aeroelastic surface.

is sufficiently over-refined ensuring the FEA yields a converged solution disregarding the amount of induced deformation and aerodynamic loading. All of these factors make the available general-purpose commercial FE packages inefficient tools when utilised for an iterative coupled aero-structure analysis of aeroelastic surfaces. The new package, consisting of a mesh generator and a FE solver, has been specially designed for this purpose. The following sections describe the strategies adopted in the development of this package making it a robust and reliable tool for coupled aero-structure analysis of aeroelastic surfaces.

## 2 High performance element

A suitable element for FEA of anisotropic fibrous composite shells must fulfil the following requirements:

1. It should be efficient and capable of giving acceptable results with coarse meshes.
2. It can be used to map 3-D curved surfaces with coarse meshes.
3. It should be able to capture the non-classical behaviours of anisotropic structures through its background theory.

The first and second requirements lead one to triangular shell elements. Flat shell elements are more attractive than the curved shell elements as the time consuming task of computing the element curvatures is completely avoided in a flat shell formulation. The cost of the stiffness formulation for a flat shell element is expected to be much less than that for a curved shell element. Hence, flat shell elements are more suitable for nonlinear and iterative analyses, as the stiffness matrix will have to be evaluated and factorised several times. Many displacement-based isoparametric flat shell elements, which have been successfully implemented in commercial packages, can be found in the literature. The third requirement suggests adopting an element based on unconventional formulation, as ordinary displacement-based isoparametric shell elements usually suffer from various kinds of locking phenomena.

Many flat shell elements based on unconventional methods such as mixed formulation, natural-mode formulation and free formulation have been successfully developed. TRIC is a triangular composite flat shell element based on natural mode formulation. It is a 3-node shear-deformable flat shell element. Its kinematics is expressed by 6 rigid-body and 12 natural straining modes of deformation. Straining modes represent axial straining, symmetrical and anti-symmetrical bending, transverse shearing and azimuth rotation modes. Inclusion of the transverse shear deformations in the formulation eliminates shear-locking phenomena based on a first-order shear deformable beam theory. A simple matrix operation transforms the elemental stiffness matrix from natural to global system of coordinates. It has been shown that it is an accurate and reliable element for analysis of thin and moderately thick anisotropic shell structures, even when using coarse meshes [3-6]. Therefore, TRIC has been selected for the FE solver part of the package as it is of the desired robustness, accuracy and efficiency and fulfils all the above requirements.

### 3 In-line semi automatic adaptive mesh generator

In the view of the earlier discussion regarding the requirement of updating the mesh in each iteration and also the fact that mesh quality becomes vital when the structure is analysed within an iteration loop, a suitable mesh generator to be used in an iterative coupled aero structure analysis should fulfil the following requirements:

1. It must account for the topology changes, automatically, in each iteration
2. It must discretize the domain, automatically, in each iteration
3. It must update the nodal loading, automatically, in each iteration
4. It should be fast
5. It should produce high quality meshes

The first three requirements lead one to take an adaptive mesh generation approach. The term adaptive meshing here refers to updating the mesh in each iteration. Adapting meshing has broadly been used by many researchers for expressing the automatic re-meshing of a domain in time marching problems with moving boundaries, or in static problems with highly deformable structures.

The third requirement also suggests an in-line mesh generator, which is located between the plugged-in aerodynamic solver and the FE solver.

When using an interactive CAD system, a twisted tapered blade/wing with variable chord and aerofoil distributions can be categorised as an object with a relatively complicated geometry. Modelling of such an object may need significant user effort and time. However, the geometry and topology of a wing or blade (chord, pre-twist, aerofoil distributions together with sizes and defining angles) can be easily defined in small and simple flat files. These files can be used to construct the model automatically with negligible computational time compared to that required for the FE solver. In an in-line mesh generation approach, the modelling part of the FEA is treated as part of mesh generation taking place prior to domain discretization.

Regarding the automated load updating, it is required to develop an interface capable of communicating with the aerodynamic solver, which is plugged into the package. The interface extracts data and calculates the nodal external forces. Depending on the method employed by the aerodynamic solver for predicting the aerodynamic forces, the results to be extracted by the interface can be in the form of load per unit span or load per unit area. When the aerodynamic solver produces aerodynamic load per unit span, e.g. when using the BEMT method for wind turbine blades, the interface should distribute the load over the shell area and then transfer it into nodal forces. Provided load per unit area, e.g. in case of using CFD or panel methods for an aircraft wing, the interface just needs to transfer it into nodal forces.

With reference to requirements 4 and 5 above, a semi-automatic mesh generation approach has been adopted, in which discretization is based on a mesh density function under the influence of the variation of the physics of the problem as well as geometrical parameters. Adopting this approach, the FEA box in Figure 1 is shown in details in Figure 2.

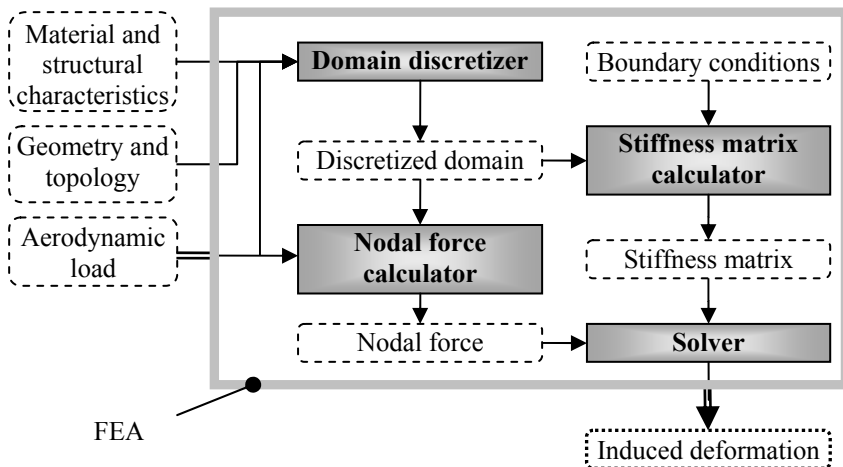


Figure 2: FEA box of Figure 1 in detail.

The following parameters affect the efficiency of a mesh when predicting the deformation, and therefore are considered in establishing the mesh density function:

1. Distributions of the dominant internal force and the effective stiffness in order to locate more deformable parts of the aeroelastic surface, avoiding over refinement of regions which are less effective in deformation.
2. The surface topological variations in order to identify the high curvature regions, as required for mapping a curved structure with flat elements.
3. Distribution of external force as required for calculating nodal forces accurately when using coarse meshes.

#### 4 Discretization strategy

Let a two-dimensional domain in the  $(\xi, \eta)$  plane is considered for discretization. Here, the mesh size at a general point  $(\xi_0, \eta_0)$  is defined as the distance between the sides of the triangle surrounding the point along two directions of  $\xi$  and  $\eta$  (Figure (3.a)). The mesh size is proportional to the inverse of mesh density function  $\rho(\xi, \eta)$ , in a directional sense, as follows:

$$\delta \propto 1 / \int_0^{\delta} (\partial \rho / \partial \xi)_{\eta=\text{const}} d\xi \quad (1)$$

$$\lambda \propto 1 / \int_0^{\lambda} (\partial \rho / \partial \eta)_{\xi=\text{const}} d\eta \quad (2)$$

It can be easily shown that:

$\forall i \in \{1, 2, \dots, n_{\xi}\}$ ; at  $\eta_0$  location

$$\int_0^{\Xi} \rho^{\xi} d\xi = \sum_{k=1}^{n_{\xi}} \int_0^{\delta_k} \rho^{\xi} d\xi = n_{\xi} (\bar{\rho}^{\xi})_i \delta_i \quad (3)$$

and  $\forall j \in \{1, 2, \dots, n_{\eta}\}$ ; at  $\xi_0$  location

$$\int_0^H \rho^{\eta} d\eta = \sum_{k=1}^{n_{\eta}} \int_0^{\lambda_k} \rho^{\eta} d\eta = n_{\eta} (\bar{\rho}^{\eta})_j \lambda_j \quad (4)$$

where,  $n_{\xi}$ ,  $\Xi$ ,  $n_{\eta}$  and  $H$  are the number of divisions and the total length of the numerical domain along  $\xi$  and  $\eta$  directions at locations  $\eta_0$  and  $\xi_0$ , and  $(\bar{\rho}^{\xi})_i = \int_0^{\delta} (\partial \rho / \partial \xi)_{\eta=\text{const}} d\xi$  and  $(\bar{\rho}^{\eta})_j = \int_0^{\lambda} (\partial \rho / \partial \eta)_{\xi=\text{const}} d\eta$  are the mean values of the mesh density over  $\delta_i$  and  $\lambda_j$  along  $\xi$  and  $\eta$  directions respectively. Generally, given a mesh density function, eqns (3) and (4) can be used for determination of the mesh size over the entire domain. In the special case of  $\partial(\partial \rho / \partial \eta) / \partial \xi = 0$ , when the variation of mesh density along  $\eta$  is independent of  $\xi$ , nodes will be located on lines parallel to  $\xi$  axis as shown in Figure 3(b). It should be noted that the mesh density is not an isotropic function and therefore  $\rho_{\xi\eta} \neq \rho_{\eta\xi}$ . Imposing this condition to the mesh density function does not affect the mesh

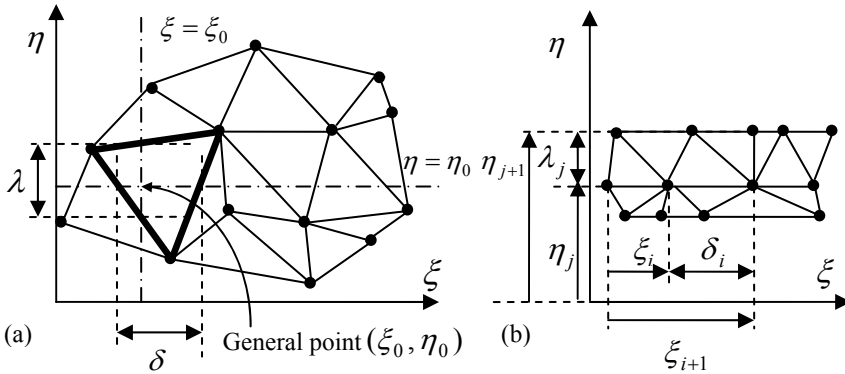


Figure 3: (a) Mesh size definition; (b) special case of parallel strips  $\rho_{\eta\xi} = 0$ .

efficiency if the physical aspects of the problem along  $\eta$  do not vary at different  $\xi$  locations. In fact, this is the case where chord and span of wing/blade are taken as the two directions in defining the mesh density function.

#### 4.1 Span-wise mesh density $\rho^s$

Since normally there is no particular region along the span of a blade/wing that the aerodynamic forces have high concentrations, there is no need to include the effect of the external forces in the span-wise mesh density. Also, typically the span-wise topological variations of the blade/wing (pre-twist, chord and aerofoil distributions) occur smoothly and therefore, since span is much longer than the chord, by generating proper elements ( $\lambda \sim \delta$ ), there is always enough span-wise strips to capture the topological variations accurately. Eliminating the effect of the external forces and the topological variations along the span leaves the dominant internal force and effective stiffness distributions as the only parameters that directly affect the span-wise mesh size. Contribution of the dominant internal force and the effective stiffness in the mesh size can be addressed by deformability density  $\rho_{def}^s$ , a dimensionless parameter bounded between 0 and 1, and defined as follows:

$$\rho_{def}^s = \frac{F/K_{eff} - F/K_{eff\ min}}{F/K_{eff\ max} - F/K_{eff\ min}} \quad (5)$$

where  $F$  is the dominant internal force and  $K_{eff}$  is the effective stiffness, relating the dominant internal force to the dominant induced deformation. Span-wise mesh density  $\rho^s$  is defined as follows:

$$\rho^s = [\rho_{def}^s]^r \quad (6)$$

Span-wise regulating exponent  $r_s \in [0,1]$  in the above equation indicates the level of dependency of the span-wise mesh density on the deformability density  $\rho_{def}^s$ . It can be either set to zero to produce a uniform span-wise mesh or manipulated automatically to prevent producing improper elements with angles smaller than a prescribed permissible smallest angle.

#### 4.2 Chord-wise mesh density $\rho^c$

In cases when no chord-wise shape change is expected, (i.e. inner fillers or the stiffeners in a blade/wing prevent the aerofoil shape from change), the deformability is not an affecting parameter in chord direction. This remains aerofoil curvature and pressure distribution (as an indicator to the chord-wise external forces) as parameters considered in constructing the chord-wise mesh density.

In the regions of high curvature, mesh must be fine enough to be able to follow the curvature. The contribution of the curvature on the chord-wise mesh size can be addressed by curvature density  $\rho_K^c$ , defined as:

$$\rho_K^c = \frac{K - K_{\min}}{K_{\max} - K_{\min}} \quad (7)$$

in which all  $K$ 's are absolute values of aerofoil curvature [7].

In high-pressure regions, there should be enough nodes in order to apply the external aerodynamic load on the blade as accurately as possible. Chord-wise force density  $\rho_F^c$  defined by the following equation represents the intensity of the pressure on the aerofoil [7].

$$\rho_F^c = \frac{C_P - C_{P\min}}{C_{P\max} - C_{P\min}} \quad (8)$$

in which  $C_P$  indicates the absolute pressure coefficient.

Direction factor  $f_D$  is a parameter that indicates how effective mesh refinement along a direction would be. In other words, it identifies those parts of the chord that are less sensitive to mesh refinement. It depends on the direction of element relative to the direction of dominant internal force. Considering the direction factor in mesh sizing reduces over refinement and improves mesh efficiency. Since the main internal force in a blade/wing is bending moment, direction factor is defined based on the angle between the normal vector to the blade surface and the bending moment vector. It should have a minimum value when the two vectors are perpendicular to each other and a maximum value when they are parallel. Here, the direction factor is defined as:

$$f_D = \left( M_{EB} \frac{dz}{dx} - M_{FB} \right) \left( \left( 1 + \left( \frac{dz}{dx} \right)^2 \right) (M_{FB}^2 + M_{EB}^2) \right)^{-0.5} \quad (9)$$



where  $M_{EB}$  and  $M_{FB}$  are the edge- and flap-wise bending moments respectively, and  $z(x)$  stands for the aerofoil contour.

To obtain chord-wise mesh density, firstly  $\rho_F^c$  and  $\rho_K^c$  are combined in a weighted sense, then direction factor  $f_D$  is applied as follow:

$$\rho^c = \left[ (r_F \rho_F^c + (1 - r_F) \rho_K^c) f_D \right]^{r_c} \quad (10)$$

$r_F \in [0,1]$  is a weighting factor representing the contribution of the force density on mesh density. Chord-wise regulating exponent  $r_c \in [0,1]$  is used to prevent the generation of improper elements by limiting the ratio of  $\delta_{\min}/\delta_{\max}$ .

## 5 Evaluation and discussion

The performance of TRIC element in stress and deformation analysis of anisotropic composite materials has been extensively studied and reported.

In order to investigate the effect of different parameters in directional mesh densities given by Equations (6) and (10), an adaptive wind turbine blade subjected to a typical aerodynamic load has been analysed. It is assumed that the skin of the blades is made of graphite/epoxy with 20 degrees off-axis mirror lay-up with a constant thickness of 10 mm through span. Mechanical properties of the blade skin are  $E_1 = 142$ ,  $E_2 = E_3 = 9.8$ ,  $G_{12} = G_{13} = 6.14$  and  $G_{23} = 4.83 \text{ GPa}$ ;  $\nu_{12} = \nu_{13} = 0.50$  and  $\nu_{23} = 0.42$ . Table 1 gives different mesh configurations used in FEA of the blade.

Figure 4 shows various convergence rates obtained from the FE analysis of the above blade by employing different mesh configurations. Here, the predicted induced twist at the tip of the blade  $\beta_{Tip}$  due to the aerodynamic loading of the first iteration has been considered for convergence study.

Table 1: Various mesh configurations.

Mesh Config.	Apply $r_c$	Apply $r_F$	Apply $f_D$	Apply $r_s$
1	Yes	No <sup>1</sup>	No <sup>3</sup>	No <sup>4</sup>
2	Yes	Yes <sup>2</sup>	No <sup>3</sup>	No <sup>4</sup>
3	Yes	Yes <sup>2</sup>	Yes	No <sup>4</sup>
4	Yes	Yes <sup>2</sup>	Yes	Yes
1. $r_F = 0$ ; chord-wise mesh size based only on the aerofoil curvature. 2. $r_F = 0.5$ . 3. $f_D = 1$ ; chord-wise mesh size based only on the aerofoil curvature and pressure distribution. 4. $r_s = 0$ ; theoretically uniform span-wise mesh size. Constraints applied on span-wise mesh size to prevent generating of improper elements.				

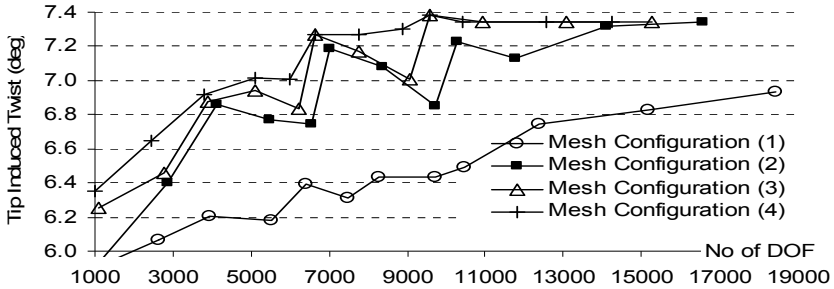


Figure 4: Effect of different parameters on the accuracy and convergence rate.

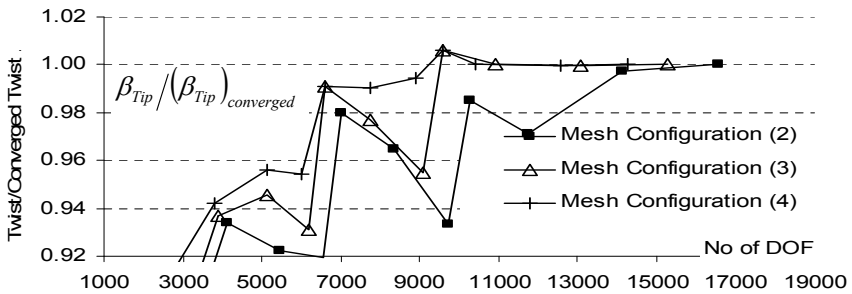


Figure 5: Effect of direction factor on the convergence rate.

According to Figure 4, the converged solution when using mesh configurations (2) and (3) is different from that of obtained by employing mesh configuration (1). This difference is due to employing the force density,  $\rho_F^e$  in the chord-wise mesh sizing, which causes gathering of nodes in high-pressure regions of the aerofoil. Therefore, the nodal loading can be calculated more accurately. The effect of employing the force density on the improvement of the convergence rate is more evident in coarser meshes with smaller numbers of chord-wise increments.

Effect of direction factor  $f_D$  on the mesh efficiency can be demonstrated by comparing the convergence rates corresponding to mesh configurations (2) and (3) in Figure 5, which is a regeneration of Figure 4. In the case of mesh configuration (2), where  $f_D$  does not contribute in mesh sizing, to obtain a solution within the margin of 4% of the converged solution  $0.98 \leq \beta_{Tip}/(\beta_{Tip})_{converged} \leq 1.02$  (or  $7.19^\circ \leq \beta_{Tip} \leq 7.49^\circ$  in Figure 4), about 13000 DOF are required. On the other hand, when the concept of direction factor as well as force and curvature densities is used in mesh creation, the required number of DOF for entering the convergence margin is approximately 9000. This shows a reduction of about 30% in the number of DOF.

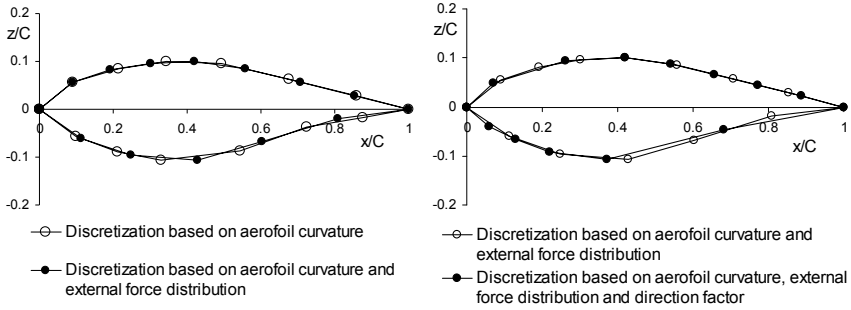


Figure 6: (a) Effect of chord-wise external force distribution on node location; (b) Node locations with and without applying direction factor.

Figure 5 also shows the effect of deformability density  $\rho_{def}^s$  on the mesh efficiency. In this case study, flap bending moment and the induced twist play the role of the dominant internal force and induced deformation respectively. These two parameters can be related to each other by the following equation (8).

$$M_{FB} = K_{eff} \partial\beta/\partial y \quad (11)$$

In this study the deformability density has been calculated through

$$\rho_{def}^s = \frac{\partial\beta/\partial y - \partial\beta/\partial y_{min}}{\partial\beta/\partial y_{max} - \partial\beta/\partial y_{min}} \quad (12)$$

in which the span-wise distribution of  $\partial\beta/\partial y$  has been calculated based on the results of the FEA of the blade from the last iteration. According to Figure 5, when the effect of the deformability of the structure is taken into account, the required DOF for entering the convergence margin reduces to less than 7000.

Figure 6(a) shows the effect of chord-wise force density on node location. One can observe that when applying force density the nodes have been shifted toward the leading edge on the upper surface, where the pressure coefficient has its higher values. Figure 6(b) shows the normalised chord-wise node locations, with and without the contribution of direction factor to the mesh size function. One can observe that due to the effect of  $f_D$ , the nodes become closer on the upper surface toward the trailing edge and on the lower surface toward the leading edge. This is due to  $f_D$  having higher values in these regions.

## 6 Conclusion

The semi-automatic adaptive mesh generator can be employed as an in-line discretizer and load updater in coupled aero-structure analysis of twisted blades and wings with several webs, variable aerofoil distribution and different material patches. The mesh size depends on the aerodynamic and structural characteristics

of the blade in chord and span directions as well as the topological characteristics. Mesh size and distribution is controlled through the number of chord-wise divisions and also five other parameters of span-wise regulating exponent (which directly affects the span-wise divisions), chord-wise regulating exponent, allowable minimum angle, force density weighting factor and the option of applying the direction factor (which affect the chord-wise mesh size directly and span-wise mesh size indirectly).

Since the domain discretization based on the presented theory includes the physics of the problem, one can anticipate more efficient meshes compared to the geometry based meshes. The results of a case study show that using force density improves the accuracy of the nodal loading when using coarse meshes and consequently increases the overall accuracy and efficiency of the aero-structure analysis. In addition, applying a direction factor can reduce the number of required DOF and taking into account the deformability of the blade can improve the convergence rate significantly. In an iterative coupled-aero-structure analysis, where the required time for FEA of an aerodynamic structure has a considerable contribution to the overall computational time, such a reduction in the number of DOF has a significant effect on its efficiency and performance.

## References

- [1] Eisler, G.R. & Veers, P.S., Parameter Optimization Applied to Use of Adaptive Blade on a Variable-Speed Wind Turbine. *Sandia National Laboratories SAND98-2668*, 1998.
- [2] Maheri, A., Noroozi, S. & Vinney, J., Application of combined analytical/FEA coupled-aero-structure simulation in design of wind turbine adaptive blades. *Renewable Energy*, **32(12)**, pp. 2011-2018, 2007.
- [3] Argyris, J., Tenek, L. & Olofsson, L., TRIC: a simple but sophisticated 3-node triangular element based on 6 rigid-body and 12 straining modes for fast computational simulations of arbitrary isotropic and laminated composite shells. *Computer Methods in Applied Mechanics and Engineering*, **145(1-2)**, pp. 11-85, 1997.
- [4] Argyris, J.H., Papadrakakis, M. & Karapitta, L., Elasto-plastic analysis of shells with the triangular element TRIC. *Computer Methods in Applied Mechanics and Engineering*, **191(33)**, pp. 3613-3636, 2002.
- [5] Argyris, J., Papadrakakis, M. & Mouroutis, Z.S., Nonlinear dynamic analysis of shells with the triangular element TRIC. *Computer Methods in Applied Mechanics and Engineering*, **192(26-27)**, pp. 3005-3038, 2003.
- [6] Maheri, A., Noroozi, S., Toomer, C., & Vinney, J., WTAB, a Computer Program for Predicting the Performance of Horizontal Axis Wind Turbines with Adaptive Blades. *Renewable Energy*, **31(11)**, pp. 1673-1685, 2006.
- [7] Maheri, A., Noroozi, S., Toomer, C., & Vinney, J., Efficient meshing of a wind turbine blade using force adaptive mesh sizing functions. *Renewable Energy*, **32(1)**, pp. 95-104, 2007.
- [8] Maheri, A., Noroozi, S. & Vinney, J., Decoupled design of wind turbine adaptive blades. *Renewable Energy*, **32(10)**, pp. 1753-1767, 2007.

